Catalyst-Free Growth of Amorphous Silicon Nanowires by Laser Ablation

F. Kokai · S. Inoue · H. Hidaka · K. Uchiyama · Y. Takahashi · A. Koshio

Abstract Amorphous silicon nanowires (NWs), 3–50 nm thick and up to 4 μm long, were grown by room-temperature continuous wave laser ablation of Si in high-pressure (0.1–0.9 MPa) Ar gas without the addition of any catalysts. The diameter and length of the NWs increased as the pressures of the ambient Ar increased. Sphere-like Si particles with diameters of 4–110 nm were observed at the tips of grown NWs and their diameters exhibited a strong correlation with the NW diameters. We propose a stress-driven self-catalytic vapor-liquid-solid mechanism to explain the growth of the NWs.

F. Kokai (✉) · S. Inoue · H. Hidaka · K. Uchiyama · A. Koshio
Division of Chemistry for Material, Graduate School of Engineering, Mie University,
1577 Kurimamachiya, Tsu, Mie 514-8507, Japan
e-mail: kokai@chem.mie-u.ac.jp
Fax: +81-59-9319422

Y. Takahashi
Division of Mechanical Engineering, Graduate School of Engineering, Mie University,
1577 Kurimamachiya, Tsu, Mie 514-8507, Japan

1 Introduction

Silicon nanowires (NWs) can be grown by various methods including laser ablation [1, 2], thermal evaporation [2, 3], and chemical vapor deposition [4]. During experiments utilizing room temperature (RT) continuous wave (cw) laser ablation aimed at growing C/Si nanostructures such as SiC nanowires and carbon nanotubes containing SiC nanowires using an Ar gas ambient with high pressures up to 0.9 MPa [5], we found we were able to grow Si NWs by ablating Si with a cw laser without the addition of any catalysts. This paper describes a simple method of synthesizing partially crystallized amorphous Si NWs by laser ablation of Si. A pressure between 0.1 and 0.9 MPa for ambient Ar was used as a dominant experimental parameter. We found that the morphology of NWs such as the length and diameter and NW fractions in deposits varied depending on the Ar pressure. In addition, the diameter distributions of NWs exhibited a strong correlation with the diameters of sphere-like Si particles observed at the ends of the Si NWs. The growth of these NWs can not be explained by previous growth mechanisms such as conventional metal-catalyzed vapor-liquid-solid (VLS) [1, 3, 4], oxide-assisted (OA) [2], or vapor-solid (VS) [6–8] mechanisms. We propose a stress-driven self-catalytic VLS mechanism for Si NW growth, where Si NWs grow from liquid-like molten Si particles at high temperature.

2 Experimental

Laser ablation of Si was carried out in the presence of Ar gas as reported in previous studies [5, 9, 10]. A Si powder (Aldrich, 99% purity and 47 μm grain size) was used and pressed into disk-plate targets (14-mm diameter and 8-mm thickness). A Si powder with higher purity (Aldrich, 99.999% purity and 250 μm grain size) was also used. A cw Nd:YAG laser (Lee Laser, Series 800, 1.06 μm wavelength and 500 W peak power) was used to ablate Si targets at RT. The laser beam was focused on the targets through a quartz window installed in a stainless-steel chamber (110 mm in diameter and 150-mm long) filled with Ar at pressures ranging from 0.1 to 0.9 MPa. The laser spot size and the power density on the target were adjusted to 2 mm and about 18 kW/cm^2, and the laser-irradiation time was set to 2 s. The laser irradiation conditions were chosen to enable stable ablation and reproducible deposition. After laser ablation using a single laser shot at different Ar pressures, the deposits in the chamber were collected and examined with a scanning electron microscope (SEM) and transmission electron microscopes (TEM) operating at 100 and 300 kV. Raman spectra of the deposits were also taken using a Raman spectrometer (Jobin Yvon, T-64000M1). Excitation (~10 μm spot) was done using 488-nm line from an Ar^+ laser. Deposits obtained after 10 laser

shots were collected and used to measure the powder x-ray diffraction (XRD) patterns on an x-ray diffractometer (Rigaku, RU-200).

3 Results and discussion

Deposits exhibiting nanoparticle and NW structures were observed depending on the Ar pressure. Figure 1 shows examples of SEM images of the deposits obtained under different Ar pressures conditions. As can be seen in Fig. 1a, particles structures with sizes of 10–100 nm were major products together with a small quantity of NWs at an Ar pressure of 0.1 MPa. As seen in the SEM images (Figs. 1b and c) of the deposits at 0.5 and 0.9 MPa, increased Ar pressure resulted in a decrease in the fraction of particle structures and efficient growth of NW structures.

Typical TEM images of the deposits at Ar pressures of 0.1, 0.5, and 0.9 MPa are shown in Fig. 2. Similar to the observation by SEM, the fraction of NWs was low at 0.1 MPa (Fig. 2a). Increased Ar pressures resulted in promoting the growth of the NWs. As seen in Figs. 2b and c, many curved NWs were able to be observed in the products formed at higher Ar pressures. Sphere-like particles were also observed at the ends of grown NWs. Unlike the reported NWs [1, 2, 6], which clearly exhibited parts with light and dark contrast corresponding to SiO_2 (or SiO_x) and Si in TEM images, our NWs did

not exhibit such parts.

We found from the observations of the SEM and TEM images that the NWs were 0.1–0.4, 0.3–0.8, and 0.8–4 μm long for Ar pressures of 0.1, 0.5, and 0.9 MPa, respectively. The NW diameter distributions obtained by measuring more than 200 samples for the three Ar pressures are shown in Fig. 3. For some NWs, as their diameters were not uniform along their directions of growth, as seen in Fig. 2, we measured them near the sphere-like particles at the tips of the NWs. The minimum diameter was 3 nm and the diameters were up to 20 nm for 0.1 MPa (Fig. 3a). The ratios of NWs with larger diameters increased for 0.5 and 0.9 MPa (Figs. 3b and c). The average NW diameters for 0.1, 0.5, and 0.9 MPa were 11.3, 18.0, and 30.2 nm, respectively. The fraction of NWs in the deposit was roughly estimated to be ~ 90% for 0.9 MPa from areas in the TEM images for several parts in the deposit.

Although the lengths and diameters of grown NWs significantly varied depending on the Ar pressure, the quality of NWs did not vary when the Ar pressure was changed. Figure 4 shows examples of high-magnification TEM images, an XRD pattern, and a Raman spectrum taken for the deposit obtained at an Ar pressure of 0.5 MPa. As can be seen in the high-magnification TEM image of a single NW with a diameter of 28.4 nm (Fig. 4a) and its tip part (Fig. 4b), NWs often exhibited a

morphology, in which a crystalline part with fringes having a ~0.31 nm spacing attributed to the Si (111) lattice plane distances [11] was in an amorphous matrix. Rings assigned to (111), (220), and (311) reflections of Si crystal and a halo pattern due to the amorphous feature were observed together in the corresponding electron diffraction pattern, as seen in the inset of Fig. 4a. There was a cladding layer around the particle (Fig. 4b). This layer may be formed due to the ununiformity of the resident density of Si atoms after the supply of Si species and the growth of a SiNW, as mentioned below. For the growth of Cu [10]- or SiC [5]-filled carbon nanotubes, Cu or SiC nanoparticles wrapped with graphitic layers were observed at the tips of the filled carbon nanotubes. The XRD pattern exhibited three diffraction lines of (111), (220), and (311) reflections that were overlapped by a broad signal (Fig. 4c). A strong band assigned to a Si-Si transverse optical (TO) phonon mode [12] was observed at 517 cm^{-1} and a weak band due to an second order TO phonon mode was also observed around 965 cm^{-1} in the Raman spectrum (Fig. 4d). The TO mode band exhibited asymmetry on its lower energy side. We note that no band due to SiO_2, which appeared at 465 cm^{-1} for SiO_2 powders (Aldrich, 99.5% purity), was observed in the Raman measurement of the deposit. Therefore, from the results of TEM, XRD, and Raman spectroscopy, we concluded that the NWs observed in this study were partially crystallized amorphous Si NWs.

To understand the possible growth mechanism for the amorphous Si NWs, we focused on the sphere-like solidified particles at the tips of grown NWs observed by TEM. We believe that the growth of NWs starts from molten particles at high temperature, similar to the NW growth in the metal-catalyzed VLS mechanism [1, 3, 4]. Although the tip structures composed of sphere-like particles and NWs attached to the particles were final structures after the growth processes had stopped, their morphologies were remarkably varied and dependent on the Ar pressures. Figure 5 shows a TEM image of several tip structures from the deposit at 0.1 MPa. Small-diameter (12.1–17.2 nm) tip particles and NWs with diameters close to those (16.5–20.8 nm) of the particles were observed. Similar tip structures can also be seen in Fig. 2a and at the bottom left of Fig. 2b. These tip structures were often observed for thinner NWs produced at lower Ar pressures. Conversely, large (37.0–103.8 nm) sphere-like particles attached with NWs with larger (17.8–51.9 nm) diameters were observed for thicker NWs produced at higher Ar gas pressures, as seen in Figs. 2b and c. However, the diameters of the thicker NWs are rather smaller than those of attached sphere-like particles unlike the close diameters of the sphere-like particles and NWs produced in lower-pressure Ar.

We measured the diameters of more than 200 samples of sphere-like particles

at the tips of NWs for the three Ar pressures of 0.1, 0.5, and 0.9 MPa (Fig. 6). Particles with small diameters of 4–40 nm existed for thin NWs grown at 0.1 MPa (Fig. 6a). As the Ar gas pressure increased, there were particles with larger diameters up to 110 nm for thick NWs grown at 0.9 MPa (Fig. 6c). The average diameters for 0.1, 0.5, and 0.9 MPa were 18.5, 24.4, and 68.2 nm, respectively. Figure 7 shows a plot of the particle diameter versus the NW diameter for 600 samples, in which both the diameters of the particles and NWs were able to be measured. As expected from the data in Figs. 3 and 6, there was a strong correlation between the particle diameter and NW diameter, while the diameter ratios of sphere-like particles and NWs differed in the tips at lower and higher Ar pressures. The correlation coefficient for all the samples was calculated to be 0.91. The correlation between smaller particles and thinner NWs was stronger because there were thin NWs with diameters close to those of the particles grown in lower-pressure Ar and there were thicker NWs with the same diameter grown from particles with largely different diameters in higher-pressure Ar.

Unlike the synthesis of Si NWs by utilizing the Fe-catalyzed VLS mechanism using a technique of pulsed laser ablation combined with an electric furnace [1], catalyst materials were not present at the tips of NWs in this study. When we used an Si powder of 99.999% purity instead of a 99% for the laser-irradiation targets, the same Si NWs

and tip structures were formed. Si targets containing Fe of more than 10 atomic % were required to grow Si NWs efficiently with the Fe-catalyzed VLS mechanism [1]. The evidence to support the OA growth mechanism was the presence of thick (>3 nm) SiO_2 cover layers around Si NWs [2]. Our Si NWs did not possess such thick SiO_2 layers, while thin natural oxidation layers most likely existed around the Si NWs due to post-oxidation. Therefore, two well-known mechanisms, i.e., those of metal-catalyzed VLS [1, 3, 4] and OA [2], could not be applied to our growth of NWs. The catalyst-free growth of Si NWs has more recently been demonstrated using thermal evaporation [6] and chemical vapor deposition [7, 8]. A VS mechanism was proposed, in which Si vapor directly deposited on the seed particles to nucleate and grow NWs. However, the involvement of liquid-like molten particles was not taken into account in the mechanism.

As a consequence, we speculate that a somewhat different driving force to nucleate Si NWs is induced in the molten Si particles, similar to the growth of one dimensional nanostructures from Si/C [5] and Cu/C [10] molten particles produced in the space confined by high-pressure Ar after cw laser ablation. The degree of confinement of ablated-species, as seen in the shadowgraphic images of laser-ablated hot species with relatively low expansion velocities of 10^2–10^3 cm/s [14], significantly

differs depending on Ar pressure, probably resulting in the formation of various types of nanostructures [5, 10]. For the high-pressure Ar of 0.9 MPa, in which the quantity of laser-ablated Si species was reduced to be less than 10% of that at 0.1 MPa estimated from the weight loss of the Si target, extreme confinement of laser-ablated Si species provides a high resident-density growth field at high temperature. We propose a mechanism, in which NWs self-catalytically grow from molten Si particles. The driving force for NW growth is the instability of the molten Si particles due to the generation of stress. First, the molten Si particles are formed depending on the resident density of Si atoms and/or small clusters confined by Ar after laser irradiation. The rapid and successive supply of Si species and their diffusion into the molten particles result in the formation of particles with high atomic densities and the generation of compressive and /or tensile stress. The diffusion and stress generation may lead to volume expansion of the molten particles. Finally, the precipitation of Si species, the formation of protrusion-like structures, and continuation of the precipitation to relieve the stress occurs from the particles leading to NW growth.

Thinner and shorter NWs grow from smaller molten Si particles in lower-pressure Ar. The low fraction of these NWs in the deposits, as seen in Figs 1a and 2a, indicates that the lower Ar pressures provide unfavorable conditions for NW growth.

This may result from the short duration available for NW growth due to rapid reduction in temperature. The observation of different tip structures, composed of sphere-like particles and NWs with different diameter ratios, between low and high pressure Ar may result from the difference in the degree of stress in the molten particles. Regardless of the lower fractions of NWs in the deposits in lower-pressure Ar, the tip structures composed of sphere-like particles and NWs with diameters close to those of the particles indicate greater precipitation of Si species relative to the volumes of the particles occurs. This may be due to a higher degree of stress induced by the rapid reduction in temperature.

Thicker and longer NWs, on the other hand, efficiently grow from larger molten Si particles in higher-pressure Ar gas. Higher resident densities of Si species may result in the growth of larger molten particles through coalescence with other molten particles, leading to thicker NW growth, in addition to a process of the molten particles enlarging caused by the supply of Si species due to the slow reduction in temperature. The temperature range that is effective for NW growth is not clear in our cw laser ablation synthesis of Si NWs, while temperatures ranging from 320 to 1260 °C have been used to grow NWs in other methods [1–4, 6–8]. Our proposed growth model including other factors such as the duration of NW growth requires further

investigations.

4 Conclusion

Si NWs (3–50 nm in diameter and 0.1–4 μm long) were successfully grown RT cw laser ablation of Si in Ar gas of 0.1–0.9 MPa without the addition of any catalysts. The growth and quantity of the NWs were significantly related to the ambient Ar pressures. Varying Ar pressure could control the diameter distribution of the NWs. Sphere-like Si particles were observed at the tips of the grown NWs and their diameters demonstrated a strong correlation with the diameters of the NWs. This novel catalyst-free growth of Si NWs was discussed in comparison with previously reported mechanisms including metal-catalyzed VLS, OA, and catalyst-free VS growth mechanisms. We proposed a stress-driven mechanism for self-catalytic VLS growth, on the basis of the formation of molten Si particles and the generation of stress due to the rapid and successive supply and diffusion of Si species into the molten particles, to explain the growth of the Si NWs.

Acknowledgements The authors gratefully acknowledge the “Kakenhi (23510128)” Grant-in-Aid for Scientific Research provided by the Japan Society for the Promotion of

Science in support of this work. This work has been partly supported by the Cooperation of Innovative Technology and Advanced Research in Evolution Area (City Area) Project of the Ministry of Education, Culture, Sports, Science, and Technology.

References

1. A.M. Morales, C.M. Lieber, Science **279**, 208 (1998)

2. N. Wang, Y.H. Tang, Y.F. Zhang, C.S. Lee, Phys. Rev. B **58**, R16024 (1998)

3. H.Z. Zhang, D.P. Yu, Y. Ding, Z.G. Bai, Q.L. Hang, S.Q. Feng, Appl. Phys. Lett. **73**, 3396 (1998)

4. J. Westwater, D.P. Gosain, S. Tomita, S. Usui, H. Ruda, J. Vac. Sci. Tech. B **15**,554 (1997)

5. F. Kokai, K. Uchiyama, T. Shimazu, A. Koshio, Appl. Phys. A **101**, 497 (2010)

6. Y. Qin, X.N. Zhang, K. Zheng, H. Li, X.D. Han, Z. Zhang, Appl. Phys. Lett. **93**, 063104 (2008)

7. B.S. Kim, T.W. Koo, J.H. Lee, D.S. Kim, Y.C. Jung, S.W. Hwang, B.L. Choi, E.K. Lee, J.M. Kim, D. Whang, Nano Lett. **9**, 864 (2009)

8. M. Cuscunà, A. Convertino, L. Mariucci, G. Fortunato, L. Felisari, G. Nicotra, C. Spinella, A. Pecora, F. Martelli, Nanotechnology **21**, 255601 (2010)

9. F. Kokai, K. Takahashi, D. Kasuya, A. Nakayama, Y. Koga, M. Yudasaka, S. Iijima, Appl. Phys. A **77**, 69 (2003)

10. F. Kokai, T. Shimazu, K. Adachi, A. Koshio, Y. Takahashi, Appl. Phys. A **97**, 55 (2009)

11. Z. Zhong, C. Yang, C.M. Lieber, *Nanosilicon*, V. Kumar Ed. (Elsevier, Oxford, 2008), pp. 176–216

12. K.W. Adu, H.R. Gutierrez, P.C. Eklund, *Nanosilicon*, V. Kumar Ed. (Elsevier, Oxford, 2008), pp. 258–288

13. W.S. Shi, H.Y. Peng, Y.F. Zheng, N. Wang, N.G. Shang, Z.W. Pan, C.S. Lee, S.T. Lee, Adv. Mater. **18**, 1343 (2000)

14. F. Kokai, K. Takahashi, M. Yudasaka, S. Iijima, Appl. Phys. A **69**, S229 (1999)

Figure captions

Fig. 1 SEM images of deposits produced at Ar gas pressures of (a) 0.1, (b) 0.5, and (c) 0.9 MPa

Fig. 2 TEM images of deposits produced at Ar gas pressures of (a) 0.1, (b) 0.5, and (c) 0.9 MPa

Fig. 3 Diameter distributions of Si NWs grown at (a) 0.1, (b) 0.5, and (c) 0.9 MPa

Fig. 4 High magnification TEM images of (a) NW and (b) tip parts of single NW, (c) powder XRD pattern, and (d) Raman spectrum of deposit obtained at 0.5 MPa. Corresponding selected area diffraction pattern is in inset of Fig. 4a

Fig. 5 TEM image with tips of Si NWs obtained at 0.1 MPa

Fig. 6 Diameter distributions of sphere-like particles at (a) 0.1, (b) 0.5, and (c) 0.9 MPa

Fig. 7 Plot of particle diameter versus NW diameter

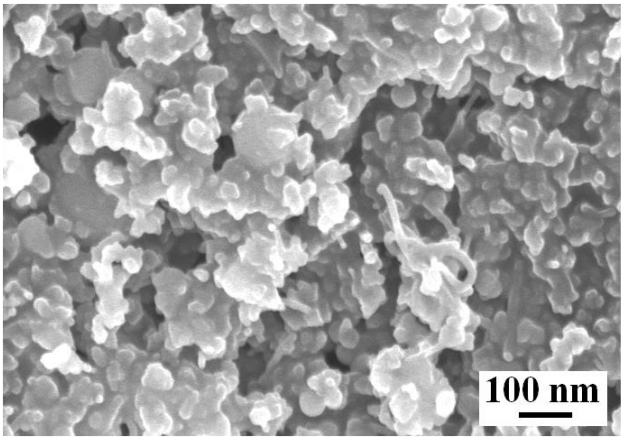

a

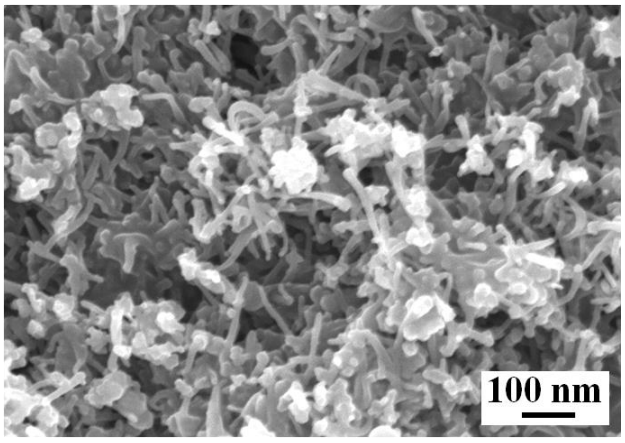

b

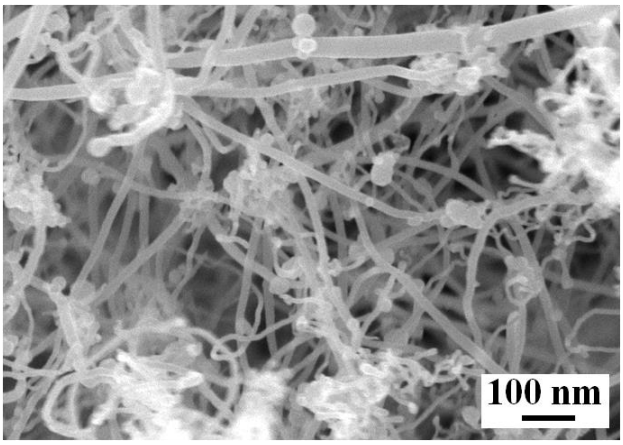

c

Fig. 1

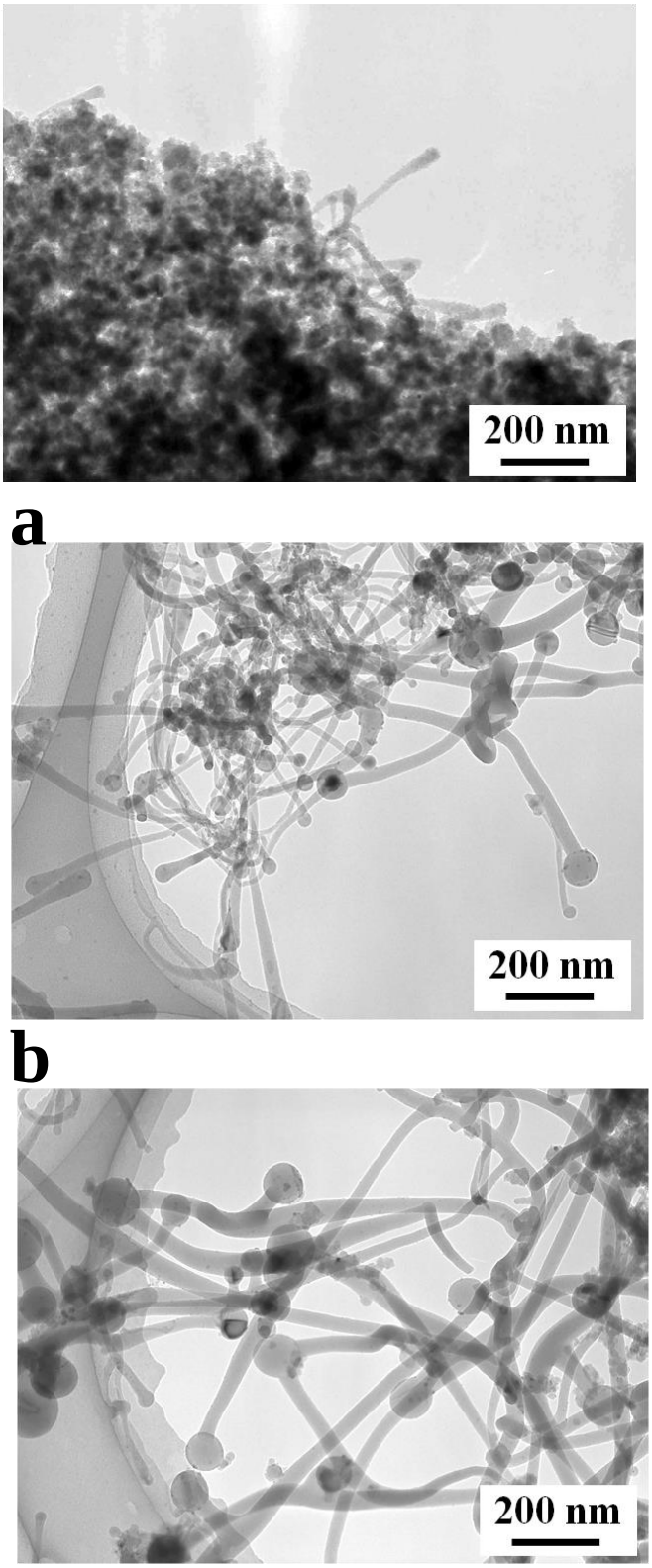

Fig. 2

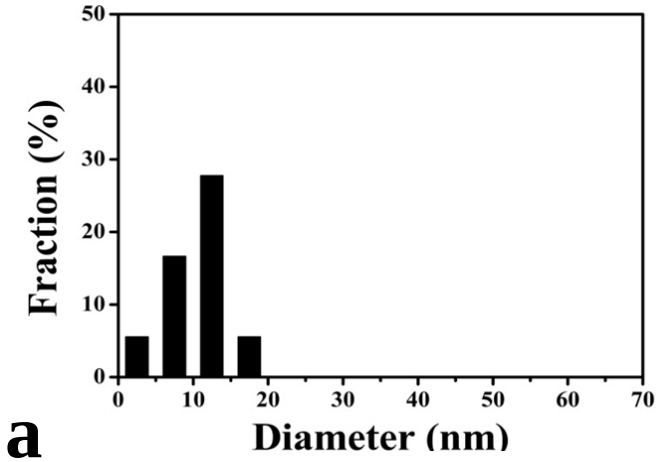
Fraction (%)
Diameter (nm)
0
10
20
30
40
50
60
70

a

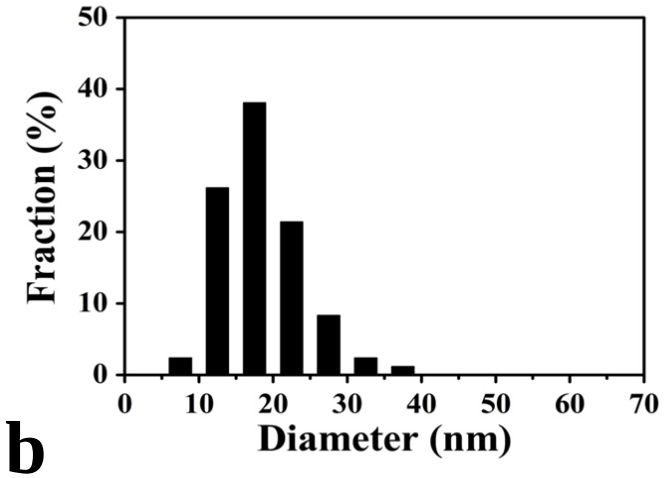
Fraction (%)
Diameter (nm)
0
10
20
30
40
50
60
70

b

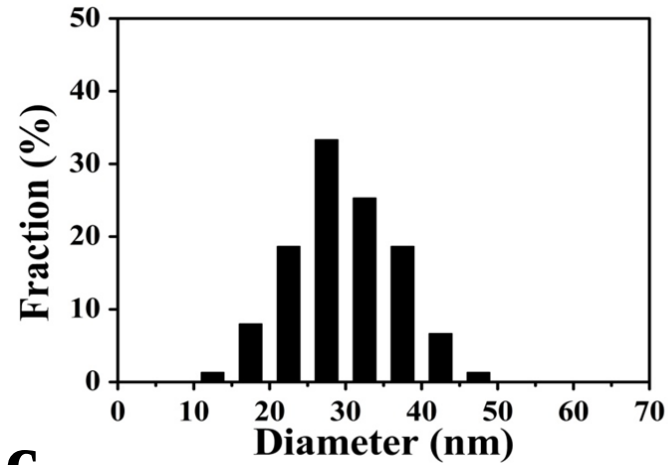
Fraction (%)
Diameter (nm)
0
10
20
30
40
50
60
70

c

Fig. 3

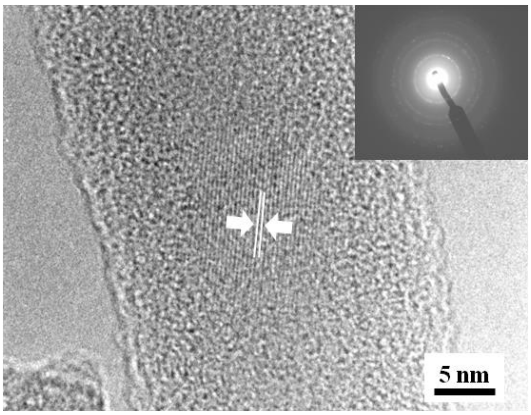
5 nm

a

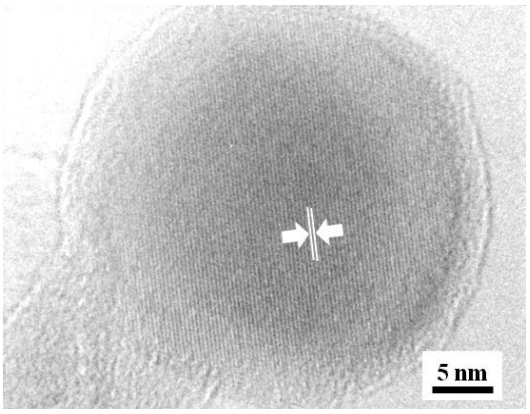
5 nm

b

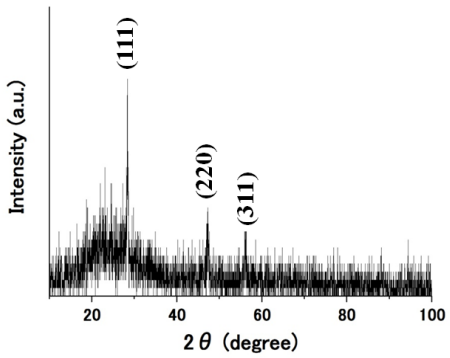
Intensity (a.u.)
(111)
(220)
(311)
20
40
60
80
100
2θ (degree)

c

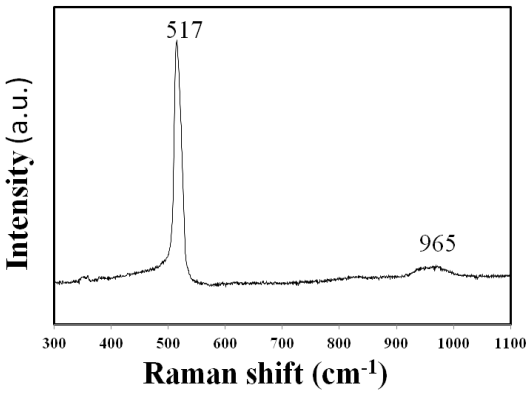
517
965
Intensity (a.u.)
300
400
500
600
700
800
900
1000
1100
Raman shift (cm-1)

d

Fig. 4

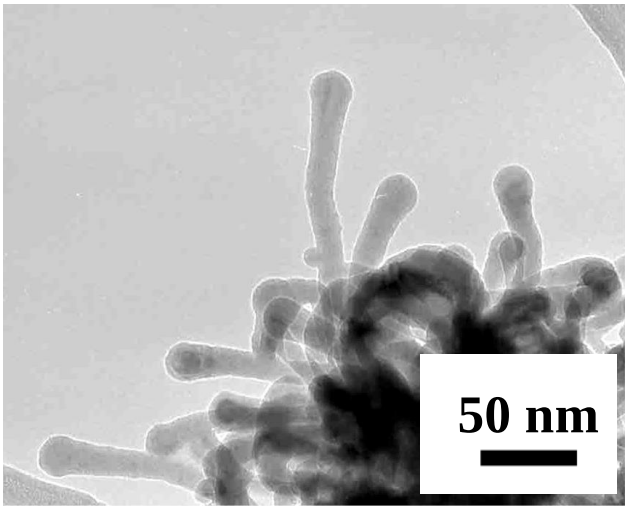

Fig. 5

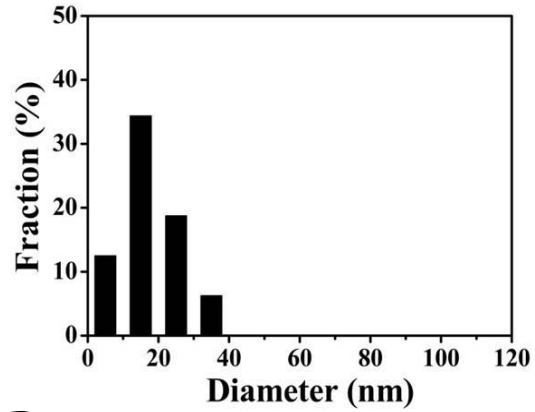
Fraction (%)
0
10
20
30
40
50
0
20
40
60
80
100
120
Diameter (nm)

a

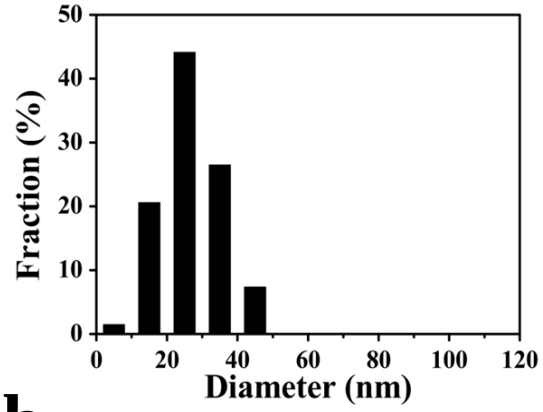
Fraction (%)
0
10
20
30
40
50
0
20
40
60
80
100
120
Diameter (nm)

b

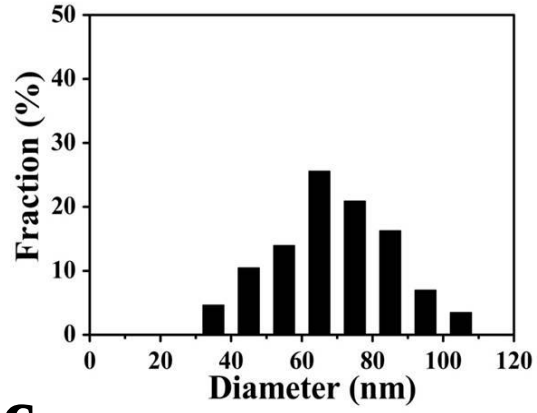
Fraction (%)
0
10
20
30
40
50
0
20
40
60
80
100
120
Diameter (nm)

c

Fig. 6

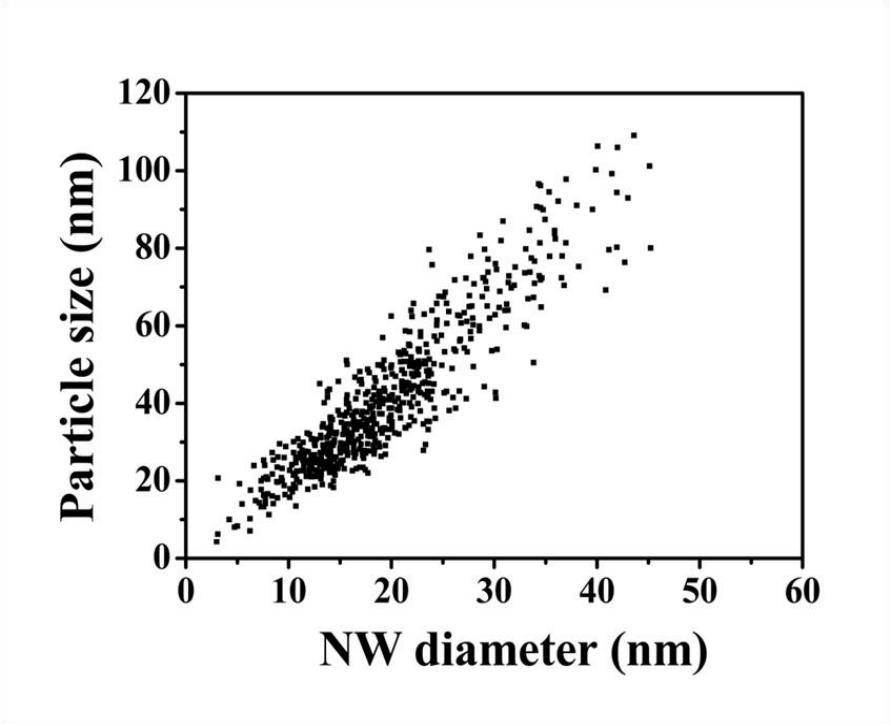
Particle size (nm)
NW diameter (nm)
0
20
40
60
80
100
120
0
10
20
30
40
50
60

Fig. 7